Supplementary online material

1 Age control

1.1 Biostratigraphy

Age models of all study sites are primarily based on biostratigraphic data, which are taken from the literature and augmented by new calcareous nannofossil data at Site 361 (section 2.1.1). The biostratigraphic zonation used in this study is based on both calcareous nannofossils and planktonic foraminifera and includes cosmopolitan taxa as well as a number of austral high latitude taxa. The austral calcareous nannofossil zonation was established by Wise and Wind (1977) and correlated against the low latitude standard zonation by Bralower (1992). The austral planktonic foraminiferal zonation was established and correlated against the standard low latitude zonation by Huber and Leckie (2011). The integrated austral biozonation scheme and its correlation against the standard low latitude biozonation is shown in Supplementary Figure 1.

Numerical ages of biostratigraphic datums of cosmopolitan taxa are taken from the GTS2012 standard timescale and were obtained through TimeScale Creator 6.8 (Gradstein et al., 2012). Numerical ages for austral taxa were obtained by linear interpolation between datum levels of cosmopolitan taxa at Site 511, which provides the most complete record and has been investigated in detail (Bralower, 1992; Bralower et al., 1994; Huber and Leckie, 2011; Wise, 1983).

We further use *Grantarhabdus coronadventis* as a biostratigraphic marker, which has its first occurrence (FO) in the earliest Aptian (Bralower et al., 1994; see also Leckie et al., 2002). According to Bralower et al. (1994), the FO of *Grantarhabdus coronadventis* postdates the FO of *Hayesites irregularis* (bottom of NC6a; 126.4 Ma), but predates the FO of *Stoverius achylosus*,

which has been placed 80% up in NC6a (at ~126.04 Ma) by Gradstein et al. (2012). We tentatively place the FO of *Grantarhabdus coronadventis* midway between these both datums and use an approximated numerical age of 126.22 Ma.

1.2 Carbon isotope stratigraphy

To refine the age models, we produced new carbon isotope records, which are correlated to a reference curve compiled by Herrle et al. (2015). The initial carbon isotope segment (CIS) assignment of the reference curve (Herrle et al., 2004) was revised according to Bottini et al. (2015) and Wissler et al. (2003) and is presented in Supplementary Figure 3a. Where possible, CIS were assigned to carbon isotope records of the study sites (Supplementary Figure 3b-f) and bottom and top ages of CIS, taken from the age model of the reference curve, were used as tie points.

2 Age models

To set up the age models, we divided all studied sediment sequences into different stratigraphically continuous segments (Supplementary Figure 3b-f). Segment boundaries are drawn at stratigraphic discontinuities that either result from unconformities or coring gaps. This segmentation provides the framework for our carbon isotope correlation. In addition, potential age ranges of each segment are used to demonstrate uncertainties in the age models. The depth and age intervals of all defined segments are reported in Supplementary Table 2. Biostratigraphic and carbon isotope tie points used to construct the age models are summarized in Supplementary Table 3. Age models were constructed by linear interpolation between tie points.

2.1 DSDP Site 361

2.1.1 New calcareous nannofossil biostratigraphy

We reinvestigated the lower part of Site 361 (cores 28 to 48) to refine the initial nannofossil zonation by Proto Decima et al. (1978). The results are presented in Supplementary Table 1. From 99 studied samples only 28 samples contain nannofossils with a predominantly poor to moderate preservation. All other samples were barren. *Hayesites irregularis* and *Eprolithus floralis,* which are the most important biostratigraphic marker species for the Early to Late Aptian interval, could be detected in sample 361-48-2 118-119 cm at 1288.18 mbsf and in sample 361-32-5 22-24 cm at 1065.22 mbsf, respectively (Supplementary Figure 2). The occurrence of *Hayesites irregularis* clearly points to an Early Aptian age of the lowermost part of the studied succession (*C. litterarius* zone). The FO of *Eprolithus floralis* indicate a late Early Aptian age and marks the boundary of the *C. litterarius*/*R. angustus* zones. In the Vocontian Basin (SE France) and Cismon Section (Italy), it occurs within the positive carbon isotope excursion of the Oceanic Anoxic Event (OAE) 1a (carbon isotope segments Ap6/Ap7; e.g., Heimhofer et al. (2004); Herrle et al. (2004)).

The upper part of the record is marked by the occurrence *Nannoconus truittii* and abundant *Eprolithus floralis* in sample 361-27-2 103-107 cm at 955.53 mbsf.

2.1.2 Age model description

Our new biostratigraphic data at Site 361 indicates that segment I extending from the bottom of the sequence to the top of core 28 comprises the *C. litterarius* nannofossil zone and parts of the *R. angustus* zone (Supplementary Figure 3b). The occurrence of *Hayesites irregularis* in core 48 provides a maximum age constraint of 126.4 Ma for segment I. Based on the biostratigraphic information, we define two CIS: (1) The $\delta^{13}C_{org}$ increase from ~-26‰ at the bottom of core 48 to

~-24‰ in core 45 (~1240 mbsf) is consistent with the carbon isotope trend during Ap1, which suggests that segment I contains (nearly) the complete *C. litterarius* zone down to the Barremain/Aptian boundary. (2) The depth interval between core 35 and 31 (1089.1 to 1050 mbsf) is characterized by a negative $\delta^{13}C_{org}$ excursion of ~4.5‰ (1089.1 to 1067 mbsf), followed by a positive excursion of ~5‰. In accordance with our new biostratigraphic data placing the FO of *Eprolithus floralis* at a depth of 1065.22 mbsf, this characteristic carbon isotope pattern most likely represents CIS Ap3-6 and thus the local expression of OAE 1a (e.g., Menegatti et al., 1998). $\delta^{13}C_{org}$ values inbetween both identified CIS (core 45 to 35) remain fairly stable at ~-25‰ VPDB, punctuated by a negative excursion of ~2‰ VPDB between 1204 and 1184 mbsf (Supplementary Figure 3b). This carbon isotope pattern cannot be correlated with confidence as the brief negative excursion has no discernable counterpart in the reference curve (Supplementary Figure 3a). However, given the identification of Ap3 further up-section and Ap1 below, we consider it most plausible that this part of the record represents Ap2. In line with the identification of Ap3-6, we furthermore assign Ap7-8 to cores 31 to 28 (1050 to 1005 mbsf), where the $\delta^{13}C_{org}$ record shows a plateau-like feature fluctuating around ~-25‰ VPDB, followed by a sharp decrease to -32‰ VPDB between 1005 mbsf and 1000 mbsf (Supplementary Figure 3b). The top of segment I lies between the FO of *Eprolithus floralis* and the FO of *Prediscosphaera columnata*, which provides only a vague minimum age estimate for segment I (i.e., <123.88 Ma; >112.95 Ma). However, considering the overall good fit between the $\delta^{13}C_{org}$ record at Site 361 and the reference curve in segment I, we consider it unlikely that the top age of segment I is substantially younger than Ap8/Ap9.

We define core 27 as segment II, which is separated from segment I by an un-cored interval between 1000 mbsf and 962.5 mbsf (Supplementary Figure 3b). Segment II falls into the *R. angustus* zone, as it postdates the FO of *Eprolithus floralis*, but predates the FO *Prediscosphaera*

columnata (Supplementary Figure 3b). An unequivocal carbon isotope correlation of segment II is difficult. However, $\delta^{13}C_{org}$ values in segment II are generally high, partly exceeding those during CIS Ap7 (Supplementary Figure 3b). Considering that segment II is younger than Ap8/Ap9, we propose that segment II spans parts of the positive carbon isotope anomaly during the Late Aptian CIS Ap13-15. This age assignment is supported by circumstantial evidences provided by biostratigraphy. The Late Aptian interval is characterized by a *Nannoconus truittii* acme during CIS 12, followed by a decline in *Nannoconus truittii* abundance and the expansion of cold water taxa during the Late Aptian Cold Spell (Ap13-Ap15; Bottini et al. (2015); Erba et al. (2015); McAnena et al. (2013)). High numbers of *Eprolithus floralis* relative to *Nannoconus truittii* found in sample 361-27-2 103-107 cm at 955.53 mbsf are indicative of cooler surface waters (e.g., Roth and Krumbach, 1986), hence supporting our age model based on our carbon isotope stratigraphy.

The FOs of *Prediscosphaera columnata* and *Hayesites albiensis* occur concurrently at the bottom of segment III (core 26), indicating that the Aptian-Albian boundary lies between core 27 and 26 (Proto Decima et al., 1978). The occurrence of *Hayesites albiensis*, which has its FO in Early Albian and its last occurrence (LO) in the Late Albian (Supplementary Figure 1), indicates that segment III is younger than 112.65 Ma and older than 110.84 Ma. Slightly lower $\delta^{13}C_{org}$ in segment III (Supplementary Figure 3b) are consistent with a global decrease in $\delta^{13}C$ towards the Early Albian (Ap16-Al3). However, an unequivocal CIS identification, and thus a more precise age assignment, is impossible.

2.2 DSDP Site 511

Sediments of Neocomian to Albian were recovered at Site 511 between in cores 49 to 62 (Basov et al., 1983). Biostratigraphic data obtained from below 534.25 mbsf yielded ambiguous age

estimates (e.g., Basov et al., 1983). Age-diagnostic calcareous nannofossils are largely absent (Wise, 1983) and stratigraphic evidence from planktonic foraminifera (Krasheninnikov and Basov, 1983), palynomorphs (Kotova, 1983), and dinoflagellates (Ludwig et al., 1983) yielded conflicting age estimates. Hence, the age of the lowest part of the sequence has broadly been classified as Neocomian (Basov et al., 1983). Our carbon isotope stratigraphic approach is unable to refine the biostratigraphic age estimate due to the lack of characteristic isotopic patterns (Supplementary Figure 3c). Therefore, we omitted the lowermost part of the sequence from further discussion.

Segment I between core 60 and 58 (534.25 to 513.65 mbsf) is of Early Aptian age as indicated by calcareous nannofossil stratigraphy placing the section into the *C. litterarius* zone (Bralower et al., 1994; Wise, 1983). A maximum age constraint of 126.22 Ma for segment I is provided by the occurrence of *Grantarhabdus coronadventis* (Bralower et al., 1994). The top of segment I is marked by a barren interval, above which the nannofossil taxa are of Late Aptian age, as indicated by the occurrence of *Eprolithus floralis* and the disappearance of *Micrantholithus hoschulzii* (Bralower et al., 1994). We use 123.88 Ma as a minimum age constraint given that the segment I predates the FO of *Eprolithus floralis*. $^{13}C_{org}$ values remain stable at ~-28‰ VPDB throughout segment I (Supplementary Figure 3c). Although this $^{13}C_{org}$ trend does not allow for an unambiguous correlation, comparison with the reference curve, which comprises several high amplitude carbon isotope fluctuations during the corresponding time interval, makes it unlikely that segment I covers CIS Ap3-6. Our preferred explanation for this discrepancy is that segment I spans parts of CIS Ap2.

At 513.65 mbsf, the $\delta^{13}C_{org}$ record shows a sharp positive shift of ~5‰ VPDB (Supplementary Figure 3c), marking the bottom of segment II (513.65 mbsf to core 49). Previous studies

interpreted this shift as the local expression of OAE 1a (Ap3-6; Jenkyns et al. (2012)). Revised foraminiferal biostratigraphy, however, indicates that the positive shift falls into the *H. trocoidea* zone (Huber and Leckie, 2011) and thus cannot be older than CIS Ap12 or 118.93 Ma. This is further supported by nannofossil data (i.e., LO of *Micrantholithus hoschulzii* at the top of segment I) indicating a Late Aptian age for the basal part of segment II (Bralower et al., 1994). Based on this biostratigraphic evidence, we conclude that CIS ~Ap3 to Ap11 are missing at DSDP Site 511 revealing a previously undescribed hiatus of ~6 Ma. We tentatively place the hiatus within the positive shift at 513.65 mbsf (Supplementary Figure 3c). $^{13}C_{org}$ values in the Late Aptian part of segment II are higher by ~5‰ VPDB compared to the segment I (tentatively interpreted as Ap2), which is overall consistent with CIS Ap12/Ap13-Ap15 (Supplementary Figure 3c).

The remainder of segment II is biostratigraphically well-dated and contains cosmopolitan Aptian and Albian calcareous nannofossils (Bralower, 1992) and planktonic foraminifera (Huber and Leckie, 2011). The Aptian/Albian boundary was placed at 486.14 mbsf at the LO of *Paraticinella eubejaouensis* (Huber and Leckie, 2011). $^{13}C_{org}$ and $^{13}C_{carb}$ records provide little additional information since carbon isotope trends during the Albian are characterized by overall low amplitude variations (Supplementary Figure 3a). High amplitude fluctuations such as OAE 1b (Ap16-18) are probably too short-lived to be resolved in our record. One feature of the $^{13}C_{carb}$ record deviating from the reference curve is a Late Aptian/Early Albian negative excursion located between 485.9 mbsf and 482.9 mbsf (Supplementary Figure 3c). However, the negative $^{13}C_{carb}$ excursion is not paralleled by a similar trend in $^{13}C_{org}$, potentially indicating a diagenetic overprint of the pristine ^{13}C signal of carbonate.

2.3 DSDP Hole 327A

Hole 327A penetrated a Neocomian to Albian sediment sequence (core 15 to 27) similar to Site 511. An undifferantiated Neocomian age was assigned to the lowermost part of the sequence below core 25 (Supplementary Figure 3d; Wise and Wind (1977)). Hence, we did not calculate numerical ages for samples from this part of the sequence.

Segment I extending from core 25 to 24 falls into the *C. litterarius* calcareous nannofossil zone as indicated by the occurrence of *Grantarhabdus coronadventis* (<126.22 Ma) and the absence of *Eprolithus floralis* (>123.88 Ma; Wise and Wind (1977)). $^{13}C_{org}$ values in core 25 and 24 are fairly invariant, similar to segment I at Site 511 ((Supplementary Figure 3d). Based on the considerations presented for Site 511, we propose that the segment I at Hole 327A likewise spans CIS Ap2 (or parts of it).

The positive carbon isotope shift, which marks the Early Aptian/Late Aptian unconformity and the boundary between segment I and II at Site 511, is not clearly visible at Hole 327A, most likely due to the lower stratigraphic resolution (i.e., 19 m coring gap between core 24 and 23). Still, $^{13}C_{org}$ values in segment II (cores 22 and 23) are increased by ~4‰ VPDB compared to segment I, consistent with the Late Aptian CIS Ap13-15 (Supplementary Figure 3d). Furthermore, the FO of *Eprolithus floralis* and the LO of *Micrantholithus hoschulzii* occur at the segment I/segment II boundary (Wise and Wind, 1977). Similar biostratigraphic trends were observed across the hiatus at Site 511. We thus conclude that a hiatus similar to that identified at Site 511 is present at Hole 327A, although its duration is biostratigraphically less well constrained as planktonic foraminiferal biostratigraphic data is lacking. The concurrency of the FO of *Eprolithus floralis* and the LO of *Micrantholithus hoschulzii* at the segment I/segment II boundary, however, indicates that the hiatus at least spans the time interval between 123.88 and

122.25 Ma. The top of segment II is defined by the FO of *Prediscosphaera columnata* between core 21 and 22 and, which marks the Aptian/Albian boundary (Wise and Wind, 1977).

The bottom of segment III (core 15 to 21) is placed at the FO *Sollasites falklandensis*, which co-occurs with the FO of *Prediscosphaera columnata* between core 21 and 22. Numerical ages for samples from segment III are obtained via linear interpolation between biostratigraphic datums as the resolution of the carbon isotope record is too low to provide further information.

2.4 ODP Hole 693A

The entire sedimentary sequence at Hole 693A (segment I: cores 44 to 51) falls into the Late Aptian *R. angustus* nannofossil zone ((Supplementary Figure 3e). An older age is unlikely due to the occurrence *Eprolithus apertior* (Mutterlose and Wise, 1990), which has a FO similar to that of *Eprolithus floralis* in the Tethys and Boreal regions and has been used as an alternative marker to define the base of the *R. angustus* nannofossil zone (Bottini and Mutterlose, 2012; Herrle and Mutterlose, 2003). The lack of typical Albian taxa, such as *Prediscosphaera columnata*, *Sollasites falklandensis*, *Tranolithus orionatus*, and *Eiffelithus turriseiffelii*, makes an age younger than Late Aptian unlikely (Mutterlose and Wise, 1990). Although a detailed planktonic foraminiferal biostratigraphy is lacking, the reported assemblages support a Late Aptian age (Leckie, 1990).

The $^{13}C_{org}$ record at Hole 693A shows a gradual decrease from ~-24‰ to ~-27‰ VPDB between bottom of the sequence to 438 mbsf followed by a stepwise increase to ~-23‰ between 438 mbsf and the top of the sequence (Supplementary Figure 3e). This trend shows a close similarity to the reference curve during the corresponding time interval, where a decline (CIS Ap8/Ap9 to Ap11), followed by a return to positive values during CIS Ap12 to Ap15 are recorded. Considering the biostratigraphic evidence for a Late Aptian age and the close similarity between the carbon

isotope record at Hole 693A and that of the reference curve, we construct the age model based on carbon isotope tuning using Ap9 to Ap13 as tie points (Supplementary Table 3).

2.5 DSDP Site 249

Early Cretaceous sediments were recovered at Site 249 (core 23 to 32). A Neocomian to Albian age was initially proposed for the sequence based on rare age-diagnostic calcareous nannofossils and foraminifera (Bukry, 1974; Sigal, 1974). Nannofossil assemblages were recently reinvestigated and extended by dinocyst biostratigraphy, revising the basal age of the sequence to Barremian (Dunay et al., 2018). The age model of Site 249 presented here is entirely based on biostratigraphy, while we will not further discuss our new carbon isotope record given the low recovery and invariant $^{13}C_{org}$ values (Supplementary Figure 3f) throughout the sequence under consideration (core 31 to 27).

An undifferentiated Early Cretaceous age has been proposed for the lowermost part of the sequence (below 393.85 mbsf) based on sparse nannoflora with a general Lower Cretaceous affinity (Dunay et al., 2018). Given this vague biostratigraphic age estimate, we do not assign numerical ages to samples from this part of the sequence.

The occurrence of the nannofossil *Bownia glabra* in core 31 (393.85 mbsf) indicates that segment I is not older than Barremian (Dunay et al., 2018). This is further supported by the occurrence of the dinocyst *Cerbia tabulata* at 390.81 mbsf (Dunay et al., 2018), which has its FO in the Barremian *P. elegans* ammonite zone in Northern Europe (Gradstein et al., 2012). We use the FO of *Cerbia tabulata* as a maximal age estimate for the segment I.

The occurrence of the nannofossil *Stoverius achylosus* in the upper part of core 28 (332.7 mbsf; Dunay et al. (2018)), provides a strong indication that the upper part of segment I has an Early Aptian or younger age. A minimum age constraint for segment I is provided by the occurrence of

Retecapsa angustiforata in cores 27 and 28, which has its LO in the Early Aptian (Bralower et al., 1994; see also Leckie et al., 2002). Gradstein et al. (2012) dates the LO of *Retecapsa angustiforata* to ~125.73 Ma (i.e., 60% up in the *D. forbesi* ammonite zone).

The cores above segment I are barren of calcareous nannofossils and lack age-diagnostic dinoflagellates (Dunay et al., 2018). Hence, samples from these cores were omitted from interpretation.

2.6 Summary

Our new chronology for South Atlantic and Southern Ocean drill sites revealed some previously undescribed features. Among others, the most noteworthy features are an Early to Late Aptian hiatus of ~6 Ma on the Falkland Plateau, the identification of OAE 1a at DSDP Site 361, and an improved stratigraphy for the crucial high latitude ODP Site 693A based on the recognition of Early to Late Aptian CIS. Still, the low stratigraphic coverage (i.e., coring gaps and low recovery) and the lack of reliable biostratigraphic information partly results in large age uncertainties. In order to address these uncertainties, we provide both the tie points used to set up our preferred age models (Supplementary Table 3) as well as the maximum and minimum age estimates for individual stratigraphic segments of the studied sequences (Supplementary Table 2). Based on these estimates, we argue that the age models are sufficiently accurate to allow cross-correlation of different study sites to the degree that multi-million year changes in water mass provenance and organic carbon burial can be traced reliably.

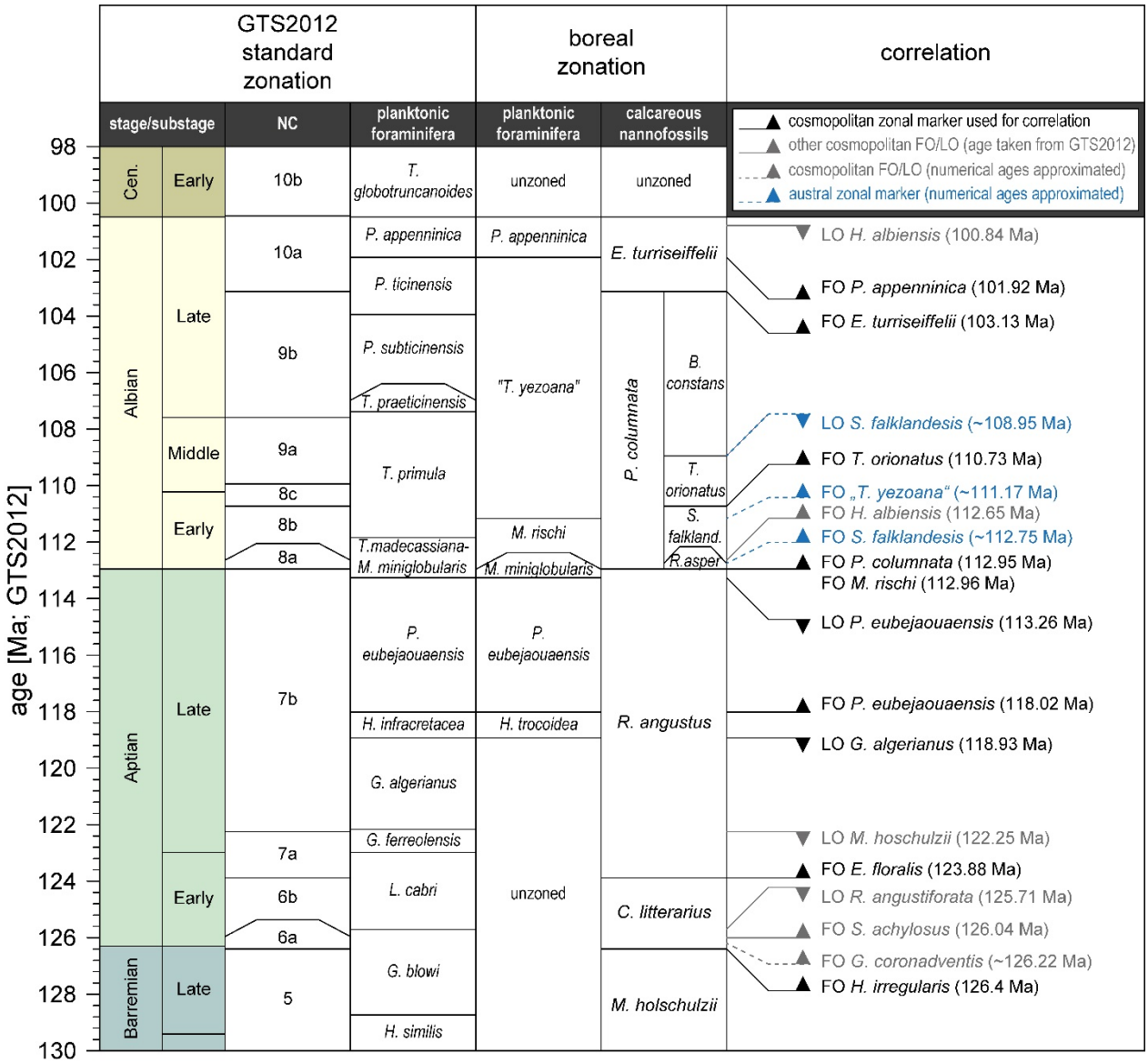

246

247 Supplementary Figure 1: Biostratigraphic scheme used in this study. Biostratigraphic datums and their

248 numerical ages used are shown on the right-hand side. Key is given in the top right corner.

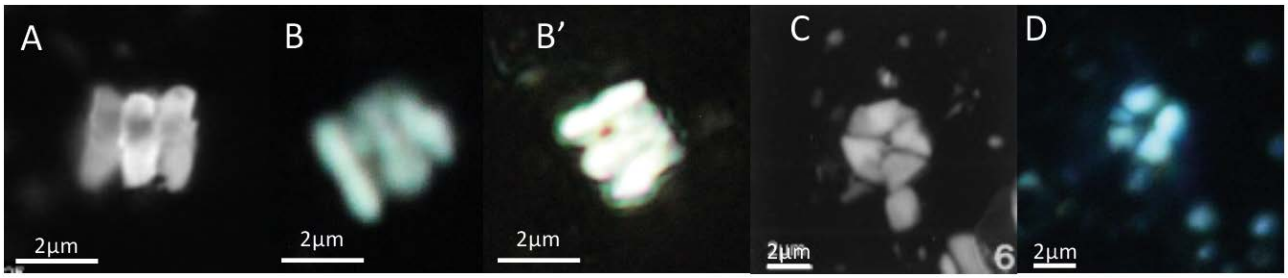

Supplementary Figure 2: Image A: *Eprolithus floralis* side view at ODP Site 198 (Bown et al., 1998). Image B and B’ *Eprolithus floralis* side view (same specimen) at DSDP Site 361 (Sample 32-5, 22 cm, 1065.22 m). Image C: *Hayesites irregularis* (Bown et al., 1998). Image D: *Hayesites irregularis* at DSDP Site 361 (sample 48-2, 118 cm, 1288.18 m).

254

255 Supplementary Table 1: Calcareous nannofossil distribution at DSDP Site 361. Preservation: b-barren p-poor, p/m-poor to moderate, m-moderate

Exp	Site	Core	Section	Top depth [m]	Bottom depth [m]	composite depth [m]	preservation	important marker species	*Chiastozygus litterarius*	*Cretarhabdus surirellus*	*Cyclagelosphaera margerelii*	*Discorhabdus ignotus*	*Diazomatholithus lehmanni*	*Hayesites irregularius*	*Eprolithus floralis*	*Lithraphidites carniolensis*	*Manivitella pemmatoidea*	*Micrantholithus hoschulzii*	*Micrantholithus obtusus*	*Nannoconus truittii*	*Rhagodiscus angustus*	*Rhagodiscus asper*	*Rhagodiscus achylostaurion*	*?Hemipodorhabdus* sp.	*Percivalia fenestrata*	*Retecapsa crenulata*	*Staurolithites* spp.	*Rotellapillus laffittei*	*Tegumentum octiformis*	*Tranolithus minimus*	*Watznaueria barnesiae*	*Zeugrhabdotus elegans*	*Zeugrhabdotus embergeri*	*Zeugrhabdotus diplogrammus*	*Zeugrhabdotus erectus*
40	361	27	2	29	33	954.79	b																												
40	361	27	2	69	71	955.19	b																												
40	361	27	2	103	107	955.53	p/m		×						×					×		×				×	×	×			×				×
40	361	27	3	19	21	956.19	b																												
40	361	27	3	54	57	956.54	b	needles																											
40	361	27	3	110	113	957.1	b																												
40	361	27	4	31	34	957.81	b																												
40	361	27	4	86	89	958.36	b																												
40	361	27	4	131	133	958.81	b																												
40	361	28	1	47	50	1000.97	b																												
40	361	28	1	86	88	1001.36	b																												
40	361	28	2	11	14	1002.11	b																												
40	361	28	2	68	71	1002.68	b																												
40	361	28	2	120	121	1003.2	b																												
40	361	28	3	28	30	1003.78	b																												
40	361	28	3	85	89	1004.35	b																												
40	361	28	3	140	141	1004.9	b																												
40	361	28	4	13	14	1005.13	b																												
40	361	28	4	77	79	1005.77	b																												
40	361	28	4	131	134	1006.31	b																												
40	361	28	5	18	19	1006.68	b																												
40	361	28	5	83	86	1007.33	b																												
40	361	28	5	138	140	1007.88	b																												
40	361	28	6	13	15	1008.13	p																								×				
40	361	28	6	60	63	1008.6	b	needles																											
40	361	28	6	128	130	1009.28	b																												
40	361	29	1	26	28	1029.26	b																												
40	361	29	1	31	33	1029.31	b																												
40	361	29	2	27	29	1030.77	b																												
40	361	29	2	75	78	1031.25	b																												
40	361	29	2	108	110	1031.58	b																												
40	361	29	3	10	12	1032.1	p																								×				
40	361	29	3	74	76	1032.74	b																												
40	361	29	4	69	71	1034.19	b																												
40	361	29	5	13	16	1035.13	p																								×				

Exp	Site	Core	Section	Top depth [m]	Bottom depth [m]	composite depth [m]	preservation	important marker species	*Chiastozygus litterarius*	*Cretarhabdus surirellus*	*Cyclagelosphaera margerelii*	*Discorhabdus ignotus*	*Diazomatholithus lehmanni*	*Hayesites irregularius*	*Eprolithus floralis*	*Lithraphidites carniolensis*	*Manivitella pemmatoidea*	*Micrantholithus hoschulzii*	*Micrantholithus obtusus*	*Nannoconus truittii*	*Rhagodiscus angustus*	*Rhagodiscus asper*	*Rhagodiscus achylostaurion*	*?Hemipodorhabdus* sp.	*Percivalia fenestrata*	*Retecapsa crenulata*	*Staurolithites* spp.	*Rotellapillus laffittei*	*Tegumentum octiformis*	*Tranolithus minimus*	*Watznaueria barnesiae*	*Zeugrhabdotus elegans*	*Zeugrhabdotus embergeri*	*Zeugrhabdotus diplogrammus*	*Zeugrhabdotus erectus*
40	361	29	5	30	32	1035.3	p															×	×							×					
40	361	29	6	65	67	1037.15	p/m		×		×						×				×	×		×		×	×				×	×	×	×	×
40	361	29	6	143	146	1037.93	b																													
40	361	30	1	52	54	1039.02	p																								×					
40	361	30	1	91	93	1039.41	p																×								×					
40	361	30	1	117	120	1039.67	b																													
40	361	30	2	49	51	1040.49	b																													
40	361	30	3	147	150	1042.97	b																													
40	361	31	1	147	149	1049.47	b																													
40	361	31	2	24	27	1049.74	p/m			×		×											×			×					×		×	×	×
40	361	31	2	91	92	1050.41	b																													
40	361	31	4	7	10	1052.57	p/m			×			×		×							×	×				×	×	×			×			×
40	361	32	1	18	20	1059.18	p																		×						×					
40	361	32	5	22	24	1065.22	p	FO *E. floralis*	×						×							×	×			×	×	×				×			×	×
40	361	32	5	67	69	1065.67	p																×		×			×				×					
40	361	32	5	132	135	1066.32	p																×				×		×			×				
40	361	32	6	37	39	1066.87	p			×	×							×	×		×	×	×	×		×		×			×		×	×	×
40	361	33	1	54	57	1067.9	b																													
40	361	33	2	143	145	1069.93	p															×	×				×				×		×			×
40	361	33	3	40	42	1070.4	b																													
40	361	33	3	63	65	1070.63	b																													
40	361	34	4	7	9	1081.07	b	needles																												
40	361	34	4	62	64	1081.62	p																								×					
40	361	34	4	85	88	1081.85	b																													
40	361	34	4	112	115	1082.12	p																								×					
40	361	35	1	143	145	1087.43	p/m																×		×		×				×		×		×	
40	361	35	2	3	5	1087.53	p																×								×					
40	361	35	3	14	16	1089.14	b																													
40	361	35	3	88	90	1089.88	b																													
40	361	36	2	48	50	1097.48	b																													
40	361	36	2	92	94	1097.92	b																													
40	361	36	2	107	109	1098.07	b																													
40	361	37	1	112	113	1106.12	p/m				×					×							×			×	×	×			×		×		×	
40	361	37	1	132	134	1106.32	p	needles																							×					
40	361	37	2	92	94	1107.42	b																													
40	361	37	2	112	114	1107.62	b																													
40	361	37	2	143	145	1107.93	b																													
40	361	38	1	91	93	1115.41	b																													
40	361	38	1	110	112	1115.6	b																													
40	361	38	2	85	86	1116.85	b																													

Exp	Site	Core	Section	Top depth [m]	Bottom depth [m]	composite depth [m]	preservation	important marker species	*Chiastozygus litterarius*	*Cretarhabdus surirellus*	*Cyclagelosphaera margerelii*	*Discorhabdus ignotus*	*Diazomatholithus lehmanni*	*Hayesites irregularius*	*Eprolithus floralis*	*Lithraphidites carniolensis*	*Manivitella pemmatoidea*	*Micrantholithus hoschulzii*	*Micrantholithus obtusus*	*Nannoconus truittii*	*Rhagodiscus angustus*	*Rhagodiscus asper*	*Rhagodiscus achylostaurion*	*?Hemipodorhabdus* sp.	*Percivalia fenestrata*	*Retecapsa crenulata*	*Staurolithites* spp.	*Rotellapillus laffittei*	*Tegumentum octiformis*	*Tranolithus minimus*	*Watznaueria barnesiae*	*Zeugrhabdotus elegans*	*Zeugrhabdotus embergeri*	*Zeugrhabdotus diplogrammus*	*Zeugrhabdotus erectus*
40	361	39	1	81	83	1124.81	b																												
40	361	40	2	79	82	1145.29	b																												
40	361	41	2	95	97	1164.45	b																												
40	361	41	3	93	95	1165.93	b																												
40	361	41	4	20	21	1166.7	b																												
40	361	42	1	8	10	1182.58	p				×												×			×	×					×		×	
40	361	42	1	63	65	1183.13	p				×												×			×	×					×		×	
40	361	42	1	112	114	1183.62	b																												
40	361	42	1	147	149	1183.97	m									×							×			×	×	×	×			×		×	×
40	361	42	6	46	47	1190.46	p/m			×																×	×	×				×	×	×	×
40	361	43	1	144	145	1201.44	b																												
40	361	43	2	8	9	1201.58	b																												
40	361	43	3	41	42	1203.41	b																												
40	361	45	2	102	103	1240.52	b																												
40	361	45	3	10	11	1241.1	b																												
40	361	45	4	31	32	1242.81	b																												
40	361	45	4	39	40	1242.89	b	needles																											
40	361	46	1	44	45	1257.44	b																												
40	361	46	2	23	25	1258.73	p							×																	×				
40	361	47	2	115	116	1269.15	b																												
40	361	47	2	133	134	1269.33	b																												
40	361	47	3	137	138	1270.87	b																												
40	361	47	4	123	124	1272.23	b	needles																											
40	361	48	2	118	119	1288.18	p	*H. irregularis*						×																					

256

257 Supplementary Table 2: Definition of stratigraphic segments at each study site used to illustrate age uncertainties

Site/ Hole	Stratigraphic segment	Bottom depth [mbsf]	Max. age estimate base [Ma]	Base defined by	Top depth [mbsf]	Min. age estimate top [Ma]	Top defined by
361	I	1295	126.4	FO *H. irregularis*	1000.5	122.16	Top Ap8
361	II	962.5	117.82	Base Ap13	953	112.95	FO *P. columnata*
361	III	915	112.65	FO *H. albiensis*	905.5	110.84	LO *H. albiensis*
511	I	534.25	126.22	FO *G. coronadventis*	513.65	123.88	FO *E. floralis*
511	II	513.65	118.93	LO *G. algerianus*	423	100.5	Alb./Cen. boundary
327A	I	431.5	126.22	FO *G. coronadventis*	381	123.88	FO *E. floralis*
327A	II	381	122.25	LO *M. hoschulzii*	326	112.95	FO *P. columnata*
327A	III	326	112.75	FO. *S. falklandensis*	175	100.5	Alb./Cen. boundary
693A	I	474.3	123.88	FO *E. apertior*	406.7	112.95	FO *P. columnata*
249	I	390.81	129.31	FO *Cerbia tabulata*	323.22	125.83	LO *R. angustiforata*

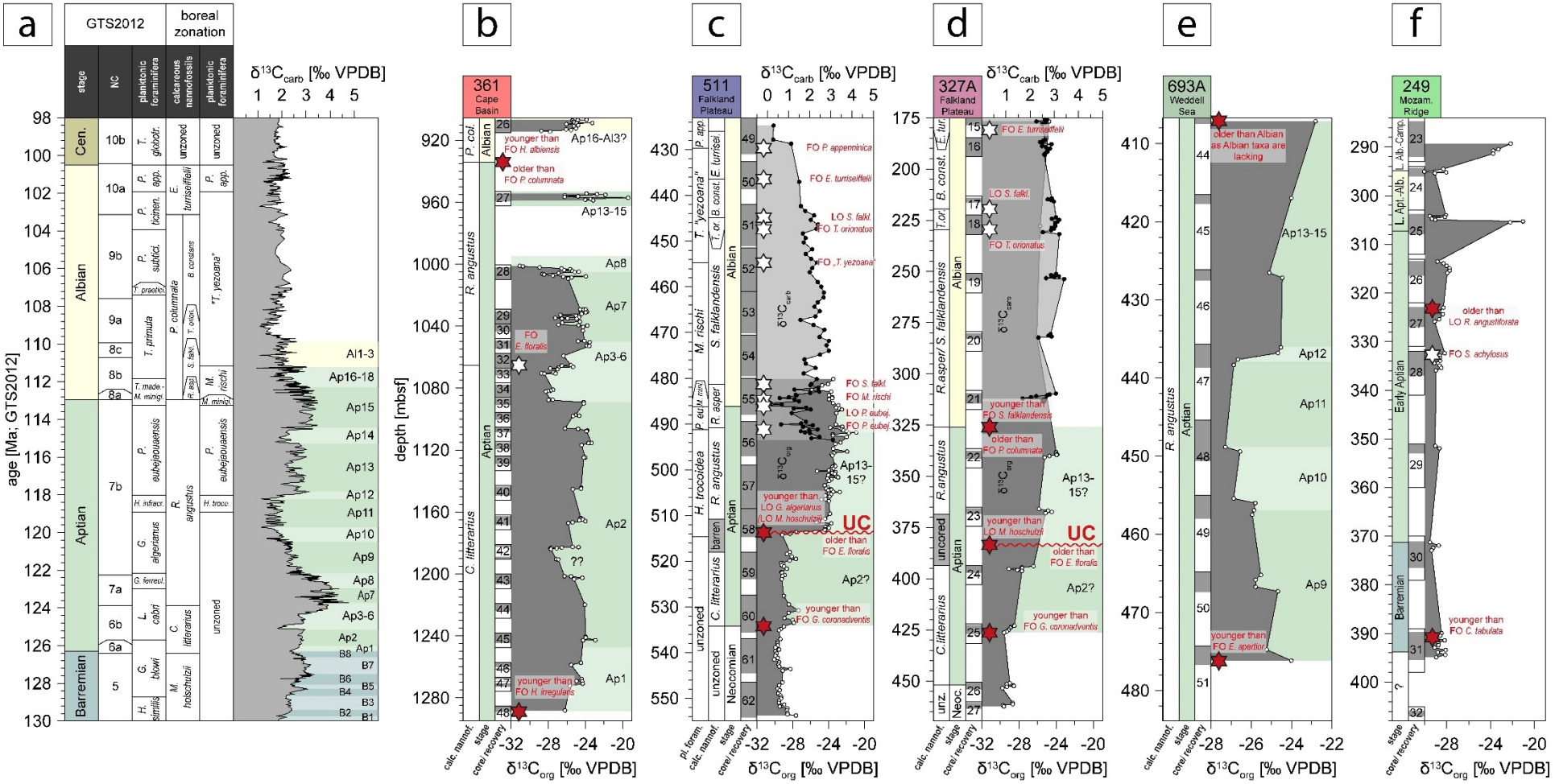

Supplementary Figure 3: (a) reference carbon isotope curve (Herrle et al., 2015) plotted against GTS2012 biozonation (Gradstein et al., 2012) and austral biozonation used in this study. Carbon isotope records (light gray: $\delta^{13}C_{carbonate}$, dark gray: $\delta^{13}C_{org}$) of (b) DSDP Site 361, (c) DSDP Site 511, (d) DSDP Hole 327A, (e) ODP Hole 693A, and (f) DSDP Site 249. Carbon isotope segments (background shading) were assigned according to Bottini et al. (2015) and Wissler et al. (2003). Numbered columns on the right denote stratigraphic segments discussed in the text with red stars representing maximum/minimum age constraints based on biostratigraphy and white stars representing additional biostratigraphic datums levels used as age model tie points. UC: unconformity

Supplementary Table 3: Tie points used to construct the age models. Ages of biostratigraphic datums are taken from the GTS2012 chronostratigraphy (Gradstein et al., 2012) or are obtained by interpolation between biostratigraphic datums of cosmopolitan taxa at DSDP Site 511 (Supplementary Figure 1). Ages of carbon isotope stratigraphic tie points are obtained from the age model of the low latitude reference curve (Herrle et al., 2015). FO: First occurrence, LO: Last occrruence, *maximum age constraint used as tie point

Site/ Hole	Type of tie point	Tie point	Depth [mbsf]	Age [Ma]	Reference
361	Biostratigraphy	FO *H. albiensis*	934	112.95	Proto Decima et al. (1978)
361	Biostratigraphy	FO *P. columnata*	934	112.65	Proto Decima et al. (1978)
361	Biostratigraphy	base Ap8	1005	122.98	This study
361	Biostratigraphy	base Ap7	1050	123.72	This study
361	Biostratigraphy	FO *E. floralis*	1065.22	123.88	This study
361	^{13}C	base Ap3-6	1089.1	125.15	This study
361	^{13}C	top Ap1	1240	126.03	This study
361	Biostratigraphy	FO *H. irregularis**	1288.18	126.40	This study
511	Biostratigraphy	FO *P. appenninica*	429.65	101.92	Huber and Leckie (2011)
511	Biostratigraphy	FO *E. turriseiffeli*	436.42	103.13	Bralower (1992)
511	Biostratigraphy	LO *S. falklandensis*	444.85	108.95	Bralower (1992)
511	Biostratigraphy	FO *T. orionatus*	447.43	110.73	Bralower (1992)
511	Biostratigraphy	FO "*T. yezoana*"	454.75	111.17	Huber and Leckie (2011)
511	Biostratigraphy	FO *S. falklandensis*	481.3	112.63	Bralower (1992)
511	Biostratigraphy	FO *M. rischi*	484.75	112.96	Bralower (1992)
511	Biostratigraphy	LO *P. eubejaouensis*	486.14	113.26	Huber and Leckie (2011)
511	Biostratigraphy	FO *P. eubejaouensis*	491.23	118.02	Huber and Leckie (2011)

Site/ Hole	Type of tie point	Tie point	Depth [mbsf]	Age [Ma]	Reference
511	Biostratigraphy	LO *L. algerianus**	513.51	118.93	Huber and Leckie (2011)
511	^{13}C	Top Ap2	513.65	125.15	This study
511	Biostratigraphy	FO *G. coronadventis**	534.25	126.22	Bralower et al. (1994)
327A	Biostratigraphy	FO *E. turriseiffeli*	181	103.13	Wise and Wind (1977)
327A	Biostratigraphy	LO *S. falklandensis*	219.5	108.95	Wise and Wind (1977)
327A	Biostratigraphy	FO *T. orionatus*	229.5	110.73	Wise and Wind (1977)
327A	Biostratigraphy	FO *S. falklandensis*	326	112.75	Wise and Wind (1977)
327A	Biostratigraphy	FO *P. columnata*	326	112.95	Wise and Wind (1977)
327A	^{13}C	Base Ap13	381	117.82	This study
327A	^{13}C	Top Ap2	393.9	125.15	This study
327A	Biostratigraphy	FO *G. coronadventis**	426.4	126.03	Wise and Wind (1977)
693A	^{13}C	base Ap13	436	117.82	This study
693A	^{13}C	base Ap12	438	118.22	This study
693A	^{13}C	base Ap11	448.8	119.72	This study
693A	^{13}C	base Ap10	456.9	120.50	This study
693A	^{13}C	base Ap9	476.2	122.16	This study
249	Biostratigraphy	LO *R. angusitforata**	323.22	125.83	Dunay et al. (2018)
249	Biostratigraphy	FO *S. achylosus**	332.70	126.04	Dunay et al. (2018)
249	Biostratigraphy	FO *C. tabulate**	390.81	129.31	Dunay et al. (2018)

270

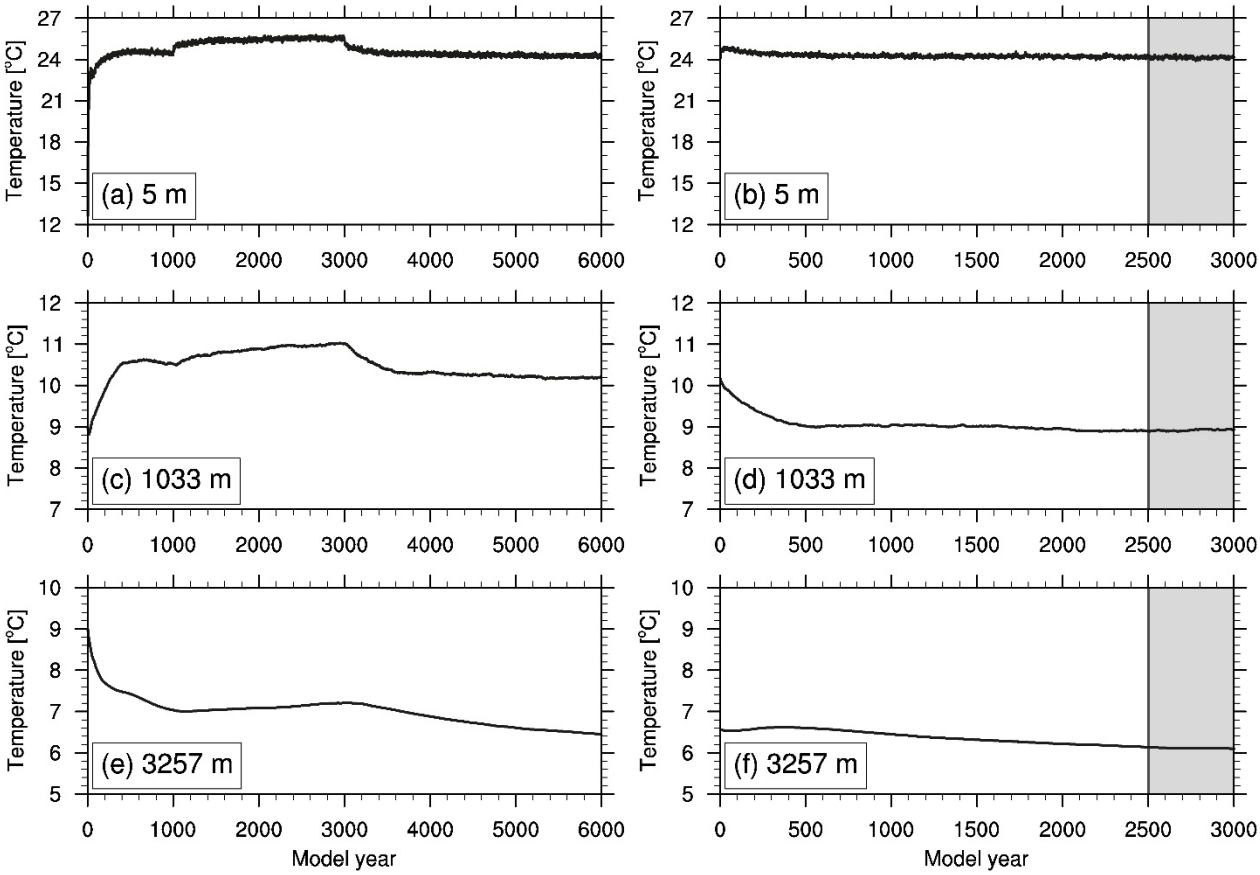

Supplementary Figure 4: Time series of globally averaged annual mean ocean temperatures in °C at 5 m, 1033 m and 3257 m. Left column shows spin-up with a slightly different model bathymetry used as initial conditions for the simulation discussed in the main text (right column). Results are averaged over the last 500 years of integration (gray boxes).

3 References

Basov, I.A., Ciesielski, P.F., Krasheninnikov, V.A., Weaver, F.M., Wise, S.W., Jr., 1983. Biostratigraphic and paleontological synthesis; Deep Sea Drilling Project Leg 71, Falkland Plateau and Argentine Basin, in: Ludwig, W.J., Krasheninnikov, V.A. (Eds.), Initial Reports of the Deep Sea Drilling Project. U.S. Government Printing Office, Washington DC, pp. 445-460.

Bottini, C., Erba, E., Tiraboschi, D., Jenkyns, H.C., Schouten, S., Sinninghe Damsté, J.S., 2015. Climate variability and ocean fertility during the Aptian Stage. Clim Past 11, 383-402.

Bottini, C., Mutterlose, J., 2012. Integrated stratigraphy of Early Aptian black shales in the Boreal Realm: calcareous nannofossil and stable isotope evidence for global and regional processes. Newsletters on Stratigraphy 45, 115-137.

Bown, P., Rutledge, D., Crux, J., Gallagher, L., 1998. Lower Cretaceous, in: Bown, P. (Ed.), Calcareous nannofossil biostratigraphy. Chapman & Hall/Kluwer Academic Publishers Group, London, pp. 86-131.

Bralower, T.J., 1992. Aptian-Albian Calcareous Nannofossil Biostratigraphy of ODP Site 763 and the Correlation Between High- and Low-Latitude Zonations, in: Duncan, R.A., Rea, D.K., Kidd, R.B., von Rad, U., Weissel, J.K. (Eds.), Synthesis of Results from Scientific Drilling in the Indian Ocean. American Geophysical Union, Washington DC, pp. 245-252.

Bralower, T.J., Arthur, M.A., Leckie, R.M., Sliter, W.V., Allard, D.J., Schlanger, S.O., 1994. Timing and paleoceanography of oceanic dysoxia/anoxia in the Late Barremian to Early Aptian (Early Cretaceous). Palaios 9, 335-369.

Bukry, D., 1974. Phytoplankton stratigraphy, offshore East Africa, Deep Sea Drilling Project Leg 25, in: Simpson, E.S.W., Schlich, R. (Eds.), Initial Reports of the Deep Sea Drilling Project. U.S. Government Printing Office, Washington DC, pp. 635-646.

Dunay, R.E., Braham, W., Cooper, M.K.E., Lester, M., Tremolada, F., 2018. Micropalaeontological dating of the basal Cretaceous section of DSDP Site 249, Leg 25, Mozambique Ridge: implications for the timing of the southern Atlantic-Indian Ocean connection. Journal of Micropalaeontology 37, 305-316.

Erba, E., Duncan, R.A., Bottini, C., Tiraboschi, D., Weissert, H., Jenkyns, H.C., Malinverno, A., 2015. Environmental consequences of Ontong Java Plateau and Kerguelen Plateau volcanism. Geological Society of America Special Papers 511, SPE511-515.

Gradstein, F.M., Ogg, J.G., Schmitz, M., Ogg, G., 2012. The Geologic Time Scale 2012. Elsevier, Amsterdam.

Heimhofer, U., Hochuli, P.A., Herrle, J.O., Andersen, N., Weissert, H., 2004. Absence of major vegetation and palaeoatmospheric pCO_2 changes associated with oceanic anoxic event 1a (Early Aptian, SE France). Earth Planet Sc Lett 223, 303-318.

Herrle, J.O., Kößler, P., Friedrich, O., Erlenkeuser, H., Hemleben, C., 2004. High-resolution carbon isotope records of the Aptian to Lower Albian from SE France and the Mazagan Plateau (DSDP Site 545): a stratigraphic tool for paleoceanographic and paleobiologic reconstruction. Earth Planet Sc Lett 218, 149-161.

Herrle, J.O., Mutterlose, J., 2003. Calcareous nannofossils from the Aptian–Lower Albian of southeast France: palaeoecological and biostratigraphic implications. Cretaceous Research 24, 1-22.

Herrle, J.O., Schröder-Adams, C.J., Davis, W., Pugh, A.T., Galloway, J.M., Fath, J., 2015. Mid-Cretaceous High Arctic stratigraphy, climate, and oceanic anoxic events. Geology 43, 403-406.

Huber, B.T., Leckie, R.M., 2011. Planktic foraminiferal species turnover across deep-sea Aptian/Albian boundary sections. J Foramin Res 41, 53-95.

Jenkyns, H.C., Schouten-Huibers, L., Schouten, S., Sinninghe Damsté, J.S., 2012. Warm Middle Jurassic–Early Cretaceous high-latitude sea-surface temperatures from the Southern Ocean. Clim Past 8, 215-226.

Kotova, I.Z., 1983. Palynological study of Upper Jurassic and Lower Cretaceous sediments, Site 511, Deep Sea Drilling Project Leg 71 (Falkland Plateau), in: Ludwig, W.J., Krasheninnikov, V.A. (Eds.), Initial Reports of the Deep Sea Drilling Project. U.S. Government Printing Office, Washington DC, pp. 879-906.

Krasheninnikov, V.A., Basov, I.A., 1983. Stratigraphy of Cretaceous sediments of the Falkland Plateau based on planktonic foraminifers, Deep Sea Drilling Project Leg 71, in: Ludwig, W.J., Krasheninnikov, V.A. (Eds.), Initial Reports of the Deep Sea Drilling Project. U.S. Government Printing Office, Washington DC, pp. 789-820.

Leckie, R.M., 1990. Middle Cretaceous planktonic foraminifers of the Antarctic margin; Hole 693A, ODP Leg 113, in: Barker, P.F., Kennett, J.P. (Eds.), Proceedings of the Ocean Drilling Program, Initial Reports. Ocean Drilling Program, College Station, pp. 319-324.

Leckie, R.M., Bralower, T.J., Cashman, R., 2002. Oceanic anoxic events and plankton evolution: Biotic response to tectonic forcing during the mid-Cretaceous. Paleoceanography 17, 1041.

Ludwig, W.J., Krasheninnikov, V.A., Basov, I.A., Bayer, U., Bloemendal, J., Bornhold, B., Ciesielski, P.F., Goldstein, E.H., Robert, C., Salloway, J., Usher, J.L., von der Dick, H., Weaver, F.M., 1983. Site 511, in: Ludwig, W.J., Krasheninnikov, V.A. (Eds.), Initial Reports of the Deep Sea Drilling Project. U.S. Government Printing Office, Washington DC, pp. 21-109.

McAnena, A., Flögel, S., Hofmann, P., Herrle, J.O., Griesand, A., Pross, J., Talbot, H.M., Rethemeyer, J., Wallmann, K., Wagner, T., 2013. Atlantic cooling associated with a marine biotic crisis during the mid-Cretaceous period. Nature Geoscience 6, 558-561.

Menegatti, A.P., Weissert, H., Brown, R.S., Tyson, R.V., Farrimond, P., Strasser, A., Caron, M., 1998. High-resolution δ13C stratigraphy through the Early Aptian "Livello selli" of the Alpine Tethys. Paleoceanography 13, 530-545.

Mutterlose, J., Wise, S.W., Jr., 1990. Lower Cretaceous nannofossil biostratigraphy of ODP Leg 113 holes 692B and 693A, continental slope off East Antarctica, Weddell Sea, in: Barker, P.F., Kennett, J.P. (Eds.), Proceedings of the Ocean Drilling Program, Initial Reports. Ocean Drilling Program, College Station, pp. 325-351.

Proto Decima, F., Medizza, F., Todesco, L., 1978. Southeastern Atlantic Leg 40 calcareous nannofossils, in: Bolli, H.M., Ryan, W.B.F. (Eds.), Initial Reports of the Deep Sea Drilling Project. U.S. Government Printing Office, Washington DC, pp. 571-634.

Roth, P.H., Krumbach, K.R., 1986. Middle Cretaceous calcareous nannofossil biogeography and preservation in the Atlantic and Indian Oceans: implications for paleoceanography. Marine Micropaleontology 10, 235-266.

Sigal, J., 1974. Comments on Leg 25 sites in relation to the Cretaceous and Paleogene stratigraphy in the eastern and southeastern Africa coast and Madagascar regional setting, in: Simpson, E.S.W., Schlich, R. (Eds.), Initial Reports of the Deep Sea Drilling Project. U.S. Government Printing Office, Washington DC, pp. 687-723.

Wise, S.W., Jr., Wind, F.H., 1977. Mesozoic and Cenozoic calcareous nannofossils recovered by DSDP Leg 36 drilling on the Falkland Plateau, Southwest Atlantic sector of the Southern Ocean, in: Barker, P.F., Dalziel, I.W.D. (Eds.), Initial Reports of the Deep Sea Drilling Project. U.S. Government Printing Office, Washington DC, pp. 269-491.

Wise, S.W.J., 1983. Mesozoic and Cenozoic calcareous nannofossils recovered by Deep Sea Drilling Project Leg 71 in the Falkland Plateau Region, Southwest Atlantic Ocean, in: Ludwig, W.J., Krasheninnikov, V.A. (Eds.), Initial Reports of the Deep Sea Drilling Project. U.S. Government Printing Office, Washington DC, pp. 481-550.

Wissler, L., Funk, H., Weissert, H., 2003. Response of Early Cretaceous carbonate platforms to changes in atmospheric carbon dioxide levels. Palaeogeography, Palaeoclimatology, Palaeoecology 200, 187-205.